Cellulose (2013) 20:1657–1667
DOI 10.1007/s10570-013-9982-7

ORIGINAL PAPER

Modification of crystallinity and pore size distribution in coagulated cellulose films

Åsa Östlund · Alexander Idström · Carina Olsson · Per Tomas Larsson · Lars Nordstierna

Received: 26 April 2013 / Accepted: 23 June 2013 / Published online: 2 July 2013

Abstract In this study the effects of altering the coagulation medium during regeneration of cellulose dissolved in the ionic liquid 1-ethyl-3-methylimidazolium acetate, were investigated using solid-state NMR spectroscopy and NMR cryoporometry. In addition, the influence of drying procedure on the structure of regenerated cellulose was studied. Complete conversion of the starting material into regenerated cellulose was seen regardless of the choice of coagulation medium. Coagulation in water predominantly formed cellulose II, whereas coagulation in alcohols mainly generated non-crystalline structures. Subsequent drying of the regenerated cellulose films, induced hornification effects in the form of irreversible aggregation. This was indicated by solid-state NMR as an increase in signal intensity originating from crystalline structures accompanied by a decrease of signal intensity originating from cellulose surfaces. This phenomenon was observed for all used coagulants in this study, but to various degrees with regard to the polarity of the coagulant. From NMR cryoporometry, it was concluded that drying induced hornification generates an increase of nano-sized pores. A bimodal pore size distribution with pore radius maxima of a few nanometers was observed, and this pattern increased as a function of drying. Additionally, cyclic drying and rewetting generated a narrow monomodal pore size pattern. This study implies that the porosity and crystallinity of regenerated cellulose can be manipulated by the choice of drying condition.

Keywords Crystallinity · NMR cryoporometry · Porosity · Regenerated cellulose · Solid-state NMR

Å. Östlund (✉) · A. Idström · L. Nordstierna
Applied Surface Chemistry, Chalmers University of Technology, Göteborg, Sweden
e-mail: asa.ostlund@chalmers.se

C. Olsson
Organic Chemistry, Chalmers University of Technology, Göteborg, Sweden

P. T. Larsson
Innventia AB, Stockholm, Sweden

P. T. Larsson
Wallenberg Wood Science Center, KTH Royal Institute of Technology, Stockholm, Sweden

Abbreviations

CI	Crystallinity index
CP/MAS	Cross polarization magic angle spinning
EMIMAc	1-Ethyl-3-methylimidazolium acetate
EtOH	Ethanol
ND	Never dried
NMMO	N-methylmorpholine-N-oxide
NMR	Nuclear magnetic resonance
OD	Oven dried
PrOH	1-Propanol
PSD	Pore size distribution
RH	Relative humidity

Introduction

Research activities regarding production of regenerated cellulose materials and textile fibers have recently intensified to respond to the global demand for alternatives to fossil-based materials and to increase the value of forest based products. The use of cellulose in its native form is traditionally found in wood based paper products and cotton based as textile fibers, whereas regeneration of cellulose allows for a range of modification possibilities with regard to the material macrostructure. Regenerated cellulose, i.e. dissolution of native cellulose followed by coagulation (precipitation), can be formed as e.g. fibers or films and be used for a variety of applications (Zhang et al. 2010). Material properties of regenerated cellulose can be altered by changing the process conditions during dissolution and coagulation (Boerstoel et al. 2001; Kotek 2006; Ziabicki 1976).

Cellulose has high potential of being more widely used in new bio-based materials and it is of value to reach a deeper understanding on how to control its morphology and structure upon regeneration. In native form the crystalline structure of cellulose is of the two allomorphs cellulose I_α or I_β. Upon mercerization or regeneration of native cellulose, cellulose II is produced. Native and mercerized/regenerated cellulose differ in term of their hydrogen bond pattern in the crystalline structure, where the former (cellulose I) has a parallel orientation of the polymers while the latter (cellulose II) has an antiparallel orientation (O'Sullivan 1997). Molecular dynamics simulations have showed that the conformation of the hydroxymethyl groups in the anhydro glucose units in cellulose differ between the two forms, which has been confirmed by X-ray diffraction (Liu et al. 2012). It was further shown that the hydroxymethyl groups in native cellulose is dominated by the trans-gauche (tg) conformation, though in regenerated cellulose the gauche-trans (gt) conformation is taking over. Interestingly, cellulose dissolved in the ionic liquid 1-ethyl-3-methylimidazolium acetate (EMIMAc) show a gt-conformation of the hydroxymethyl group, possibly aiding in the cellulose I to cellulose II transformation during coagulation (Liu et al. 2012).

The conversion from native to regenerated cellulose cannot be reversed, revealing that cellulose II is thermodynamically more stable than cellulose I (O'Sullivan 1997). The stability of cellulose II seems to be governed by an increased hydrophobicity of one of its crystal planes (Cousins and Brown 1995; French et al. 1993). Moreover, Isobe et al. (2012) have confirmed experimentally that the route for cellulose gelation, which occurs by heating a solution of cellulose in alkali, is a two-step process: primarily by ring-stacking of the anhydro glucose unit driven by hydrophobic interactions forming monomolecular sheets; secondly by intermolecular hydrogen bonding (Isobe et al. 2012).

During the coagulation process, properties of the formed cellulose are tunable by choice of conditions such as temperature and coagulation medium. Both these properties strongly affect the interaction between the polymer and its solvent (Laity et al. 2002). From our view, there is a relationship between the dissolution and the regeneration of cellulose: as the mechanism of dissolving cellulose is dependent on the choice of solvent, these mechanisms are explaining the driving forces during aggregation of cellulose depend on the choice of coagulant. Coagulation liquids of different polarity (e.g. polarity index from low to high: pentane < propanol < acetone < ethanol < water) can be used to control the morphology of the regenerated material, as increased polarity of the coagulant governs the hydrophobic interactions between the polymer chains during regeneration. This hypothesis is based on the amphiphilic property of the polymer (Lindman et al. 2010), which would interact differently depending on the polarity of the coagulant, as the miscibility of solvent and coagulant play a role. Isobe et al. (2011) showed that cellulose, dissolved in LiOH/H_2O/urea and precipitated in various coagulation media with increasing polarity (acetone < EtOH < MeOH < aqueous solutions of Na_2SO_4 and H_2SO_4), regenerates into a more ordered cellulose. One view on the coagulation mechanism for cellulose dissolved in non-derivatizing solvents is as a Fickian-diffusion controlled process, describing the change in diffusion coefficients during gelation of the sample (Biganska and Navard 2005). This suggests a two-step regeneration where the coagulant first dilutes the solvent, and then removes the rest of the solvent bound to cellulose, which leaves the polymers in the solution to be spatially homogeneously distributed followed by phase separation via spinodal decomposition (Biganska and Navard 2009). This has been shown to be valid for regenerated material from different ionic solvents such as NaOH/H_2O, N-methylmorpholine-N-oxide monohydrate (NMMO), and EMIMAc (Biganska

and Navard 2009; Sescousse et al. 2011). The theory further supports slow coagulation at low miscibility of the cellulose solvent in the coagulation medium, which occurs at lower polarity of the coagulant when using highly charged solvent for cellulose. In addition, when the cellulose is regenerated into a hydrogel, porosity and crystallinity may be tuned by, for instance exposing the samples to pressure (Liu and Budtova 2012; Yang et al. 2012).

In this work the effects of altering the coagulation media and drying conditions of regenerated cellulose, herein as a hydrogel film, have been investigated with NMR cryoporometry and solid-state NMR spectroscopy. The water-swollen state of the cellulose films and the effect of drying films by various methods were investigated with regard to porosity and crystallinity. The combination of the two NMR techniques allowed for a study of the changes in pore size distribution (PSD) in the water-swollen state and the variation in polymorphous structures upon the effect of choice of coagulant, i.e. coagulation speed, and drying conditions. This generates information about the structural differences of the material on a nanometer level that may be reflected in the mechanical properties and reactivity of the material.

Materials and methods

Materials

The pulp used was a never dried commercial 96α *Eucalyptus* dissolving pulp produced by Sappi at the Saiccor mill, South Africa Nocanda et al. (2007). 1-Ethyl-3-methylimidazolium acetate (EMIMAc, 97 %), ethanol (EtOH, 95 %), 1-propanol (PrOH, 99 %), LiCl (≥98 %), and NaCl (≥99 %) were all purchased from Sigma Aldrich and used as received. All water used was of deionized grade.

Preparation of cellulose films

Solutions of 4 wt% never dried pulp in EMIMAc were prepared by evaporation of excessive water in an oven at 60 °C over night, followed by continuous stirring of the pulp/EMIMAc solution for 2 h at 60 °C to reach a complete dissolution. Cellulose films were then prepared by coagulating the cellulose at room temperature in one of three different coagulation media: H_2O, EtOH, or PrOH respectively. The coagulation procedure was as follows: 2.0 g of heated cellulose solution was pressed between two Petri dishes (diameter 80 mm) in order to generate samples with equal diameter. The two Petri dishes, with cellulose solution in-between, were separated and immersed into a coagulation bath where the cellulose was allowed to coagulate and self-detach from the dishes which were then removed. Using this preparation setup for the cellulose films, the size and thickness of the films were kept constant. After being rinsed two times in fresh coagulation media (i.e. H_2O, EtOH, or PrOH respectively), the final washing step was performed in water to ensure that neither coagulant nor EMIMAc residues remained in the samples. The macrostructure was assumed to be given predominantly during the first coagulation step, why removing residuals of EMIMAc and the coagulation medium by washing with water is believed to affect the films to a lesser extent.

Drying conditions

The films coagulated in H_2O were dried using different drying strategies. A set of films was prepared according to Table 1. The never dried films (ND) were used as reference material. Two films were placed in desiccators with controlled relative humidity (RH) for more than 1 week to ensure equilibrium. Two salts were used to control the relative humidity; NaCl and LiCl giving 75 and 11 % RH respectively. One set of films was oven dried at 105 °C for 1 h (OD) and one

Table 1 Overview of the five different drying strategies

Sample name	Coagulation medium	Drying strategy
H_2O ND	H_2O	Never dried films (reference material)
H_2O 75 % RH	H_2O	Films dried at 75 % RH for 3 weeks
H_2O 11 % RH	H_2O	Films dried at 11 % RH for 3 weeks
H_2O OD	H_2O	Films dried in oven at 105 °C for 1 h
H_2O 5 × OD	H_2O	Films dried in oven five times at 105 °C for 1 h

set of films were subjected to five cycles of repeated drying in oven (5 × OD). Before each cycle the films were submerged and centrifuged in water at 3,000*g* for 15 min after which the excess water (supernatant) was removed. Films coagulated in EtOH and PrOH were also subjected to identical treatment and drying strategies as here described for H_2O-coagulated films.

Solid-state NMR spectroscopy

To ensure that all samples were treated uniformly, prior to solid-state NMR measurements all samples were submerged in water and centrifuged at 3,000*g* for 15 min. The samples were then packed, in wet state, directly in the solid-state rotor.

All solid-state NMR experiments were performed on a Varian Inova-600 operating at 14.7 T, equipped with a solid-state probe with rotor diameter of 3.2 mm. Measurements were conducted at 298 K with a magic angle spinning (MAS) rate of 15 kHz. The CP/MAS ^{13}C-NMR-spectra were recorded using a cross polarization (CP) pulse sequence followed by a SPINAL64 ^{1}H decoupling during acquisition. Optimized acquisition parameters included a 2.9 μs ^{1}H 90° pulse, 1,100 μs contact time, 35 ms acquisition time, 5 s recycle delay to allow for complete thermal equilibrium, and 16,384 acquisitions for each spectrum. The solid-state NMR spectra were processed and deconvoluted in MestreNova 7.0.3 software with 8,192 points zero-filling, phase correction, and a first order polynomial baseline correction in the processing. Exponential apodization of 30 Hz was applied to reduce noise levels. The entire integral, between 112 and 56 ppm, of each spectrum was normalized in order to be able to follow signal intensity changes when applying different drying environments. This range was chosen to include all signals for cellulose.

The signals from the C-4 atoms in cellulose II give rise to a cluster of signals in the 90–80 ppm spectral region, which can be modeled as originating from six signals of separate origin, as illustrated in Fig. 1. Two signals, at 89.3 and 88.1 ppm, have been interpreted as originating from crystalline cellulose II (Newman and Davidson 2004). A narrow signal at 86.6 ppm was assigned to C-4 atoms located in polymers residing on the cellulose II crystal surfaces and a broad signal at about 84.2 ppm was assigned to cellulose in disordered regions (Ibbett et al. 2007). An additional narrow signal at 85.1 ppm, not previously seen in earlier work, was tentatively assigned to origin from C-4 atoms on cellulose II crystal surfaces (Zuckerstätter et al. 2013), as an accompanying signal. In addition, a signal at 82.5 ppm was assigned to origin from low molecular mass *β*-(1,4)-D-glucan polymers or xylans. The chemical shift was set according to the assignment by Newman (2004).

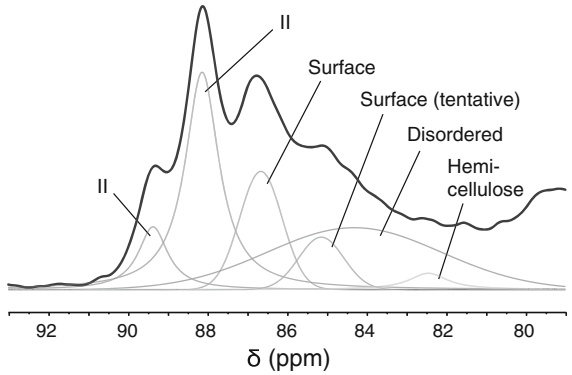

Fig. 1 Deconvolution of the solid-state CP/MAS ^{13}C NMR C-4 signals, using the theory by Zuckerstätter et al. (2013), of cellulose *II* of a never dried film precipitated in water

To obtain quantitative information of various NMR peaks in the CP/MAS spectrum, e.g. crystallinity index (CI), certain conditions has to be fulfilled in order to ensure that the signal intensity is directly proportional to amount present in the sample. Relative signal intensities must be preserved during cross-polarization. Therefore, relative signal intensities were recorded for an array of cross-polarization times in a manner similar to the study performed by Larsson et al. (1997), though without the addition of an internal standard. It was found that the ratio between the sum of signal intensity originating from crystalline cellulose II (89.3 and 88.1 ppm) and the sum of signal intensity originating from non-crystalline cellulose forms (86.6, 85.1, 84.2, 82.5 ppm) remained constant for contact times between 600 and 2,000 μs. A contact time of 1,100 μs was judged suitable for all samples.

Cellulose II CI was calculated by using two reference samples with known crystallinity, one with cellulose I and one with cellulose II, as standard samples. The crystallinity of the reference samples were determined by an X-ray diffraction peak height method (Park et al. 2010). The entire spectral integrals, between 112 and 56 ppm of the solid-state NMR spectra of the two samples, were normalized and two regions with regard to the chemical shift were

chosen, 65.5–65.7 and 107.5–107.7 ppm, corresponding to separate signals from cellulose I and cellulose II, respectively. Samples with unknown CI prepared in the current study were then normalized and integrated in an equivalent manner and by comparing the integral values obtained with those acquired from the reference samples the cellulose II CI was estimated. The error of the method was estimated by comparing the CI obtained using the above method, to CI obtained from C-4 deconvolution (Park et al. 2009), which then generates an error of ±4 % with regard to CI.

NMR Cryoporometry

Cellulose films, obtained after the different drying strategies (Table 1), were centrifuged at 3,000*g* for 15 min in separate centrifugation tubes with excessive water to ensure that all pores were completely filled with liquid. After placing the sample materials in individual NMR tubes, water was added to ensure the presence of a small amount of bulk water, and the NMR tubes were sealed. Each sample contained approximately 10 mg pulp and 60 mg water. The ^{1}H NMR signal was recorded on a Bruker Avance 600 spectrometer equipped with a TXI 5-mm probe head, running with cooled nitrogen as cooling gas and a BTU 3000 temperature control unit with precision of ±0.1 °C. A CPMG pulse sequence was used, $(90^{\circ}_{x} - \{\delta - 180^{\circ}_{y} - \delta\}_{n} - \text{acquisition})$, where the relaxation delay parameters were set to $\delta = 0.2$ ms and the CPMG pulse train loop four times ($n = 4$) prior to each acquisition. This provided a total transverse relaxation delay ($\Delta = 2\ \delta\ n$) of 1.6 ms to ensure minimal suppression of signal from liquid water and complete suppression of signals from both cellulose material and frozen water. The measurement was performed by first decreasing the temperature to −44.2 °C in order to completely freeze the sample, followed by increasing the temperature stepwise by 5 °C up to −14.2 °C, then from −14.2 to −4.2 using a temperature step of 1 °C, from −4.2 to −1.0 using a temperature step of 0.2 °C, and from −1.0 to bulk melting temperature using a temperature step of 0.1 °C. At each increment the signals were recorded after establishment of thermal equilibrium, normally achieved by a waiting time from 20 min to 2 h depending on the amount of water in the corresponding pore size range.

To minimize possible errors in signal intensity due to Curie's law, i.e. increase in NMR signal intensity by decreased temperature, and/or due to changes in sensitivity in the probe, the recorded signals were compensated from control measurements with n-pentanol (Petrov and Furó 2009). The signal for n-pentanol, with freezing point (−79 °C) well below the relevant temperature range for this study, was recorded from −44.2 °C to 0 °C showing a linear relationship in the signal-temperature dependence to be corrected for in the cryoporometry experiments.

The melting point depression, ΔT, is related to the pore radius, r, via the bulk properties of the probe liquid, K, as described by the Gibbs–Thomson equation

$$\Delta T \propto -\frac{K}{r-\tau}$$

where K is 25 nm for water and τ represents the thickness of a pre-molten liquid-like layer on the surface of the substrate, here assumed constant with regard to temperature and two monolayers thick i.e. 0.6 nm (Boissier et al. 2012).

Results and discussion

Impact of coagulation medium

Figure 2 shows the solid-state NMR spectra of the regenerated starting materials H_2O ND, EtOH ND,

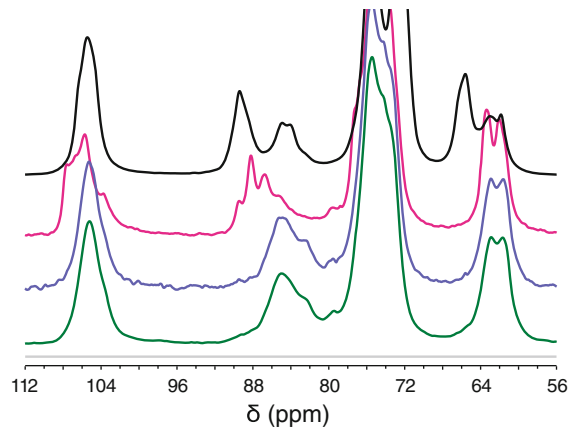

Fig. 2 Solid-state CP/MAS ^{13}C NMR spectra of cellulose. *From the top* pulp (*black*), the regenerated cellulose films after coagulation in H_2O (*pink*), EtOH (*blue*), and PrOH (*green*). (Color figure online)

and PrOH ND respectively, together with the original pulp spectrum.

Complete conversion from initial cellulose I to cellulose II and/or non-crystalline cellulose was detected for all regenerated samples. For films coagulated in H_2O a higher degree of cellulose II was found compared to the films coagulated in EtOH and PrOH, where only minor amounts of cellulose II were present. For the major part of the latter samples NMR signals originating from non-crystalline regions were detected. Similar results have been observed in previous studies (Mori et al. 2012). The inhibited conversion to cellulose II in alcohols can be explained by a decreased preference of the EMIMAc to diffuse into the coagulation media. When using H_2O as coagulation medium, a relative fast exchange of the solvent would occur, compared to a slow exchange of solvent when using EtOH or PrOH as coagulation medium. As mentioned in the "Introduction", by using molecular dynamics simulations, Liu et al. (2012) investigated the dissolution of cellulose I_β in EMIMAc, showing that the cellulose in EMIMAc had the hydroxymethyl group in the gt-position, same conformation as in cellulose II (Liu et al. 2012). In a protic solvent, such as water or an alcohol, the hydroxymethyl group was found to be in the gg-position. One interpretation can be that during a fast solvent exchange the hydroxymethyl group will be trapped in the gt-conformation, which could be beneficial for the formation of cellulose II. During a slower solvent exchange, e.g. when EtOH or PrOH is used as coagulation medium, the hydroxymethyl group can change conformation to a more energetically favorable one. The lower solubility for EMIMAc in EtOH and PrOH, compared to water, can therefore explain the change of conformation as was seen in the final product. The low solubility was also the reason why the final washing step was conducted with water, as residual EMIMAc was found in films prepared without the final washing step.

Impact of drying

The C4 region of the solid-state NMR spectra recorded on samples after application of the different drying strategies on films coagulated in H_2O is shown in Fig. 3. An apparent increase of crystalline signal intensity (a and b) at 89.3 and 88.1 ppm (Zuckerstätter et al. 2009) and a slight decrease of non-crystalline signal intensity (c and d) at 86.6 and 85.1 ppm were detected when applying more intense drying methods.

By applying the assignment by Zuckerstätter et al. (2013), where the signals at 86.6 and 85.1 ppm origin from surfaces, this behavior can be interpreted that

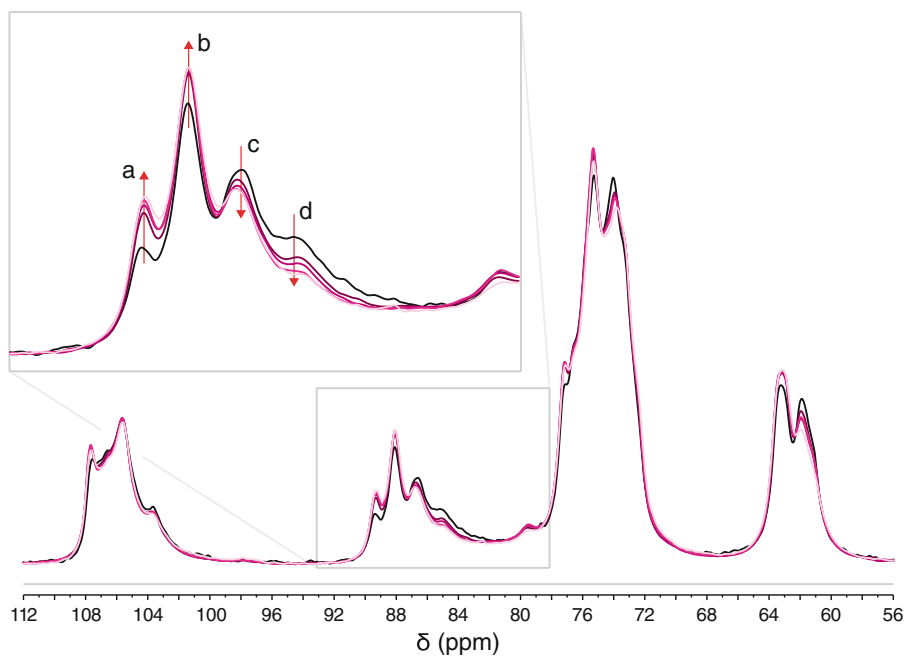

Fig. 3 Solid-state CP/MAS ^{13}C NMR spectra of the films coagulated in H_2O: ND (*black*), 75 % RH (*violet*), 11 % RH (*dark pink*), OD (*pink*), and 5 × OD (*light pink*). The C-4 region is enlarged and the *arrows* are highlighting the turnover of the spectra. (Color figure online)

NMR signal from atoms on non-crystalline surface decreases in exchange to signals with origin from crystalline material. This result indicates that regenerated cellulose shows a similar behavior as native cellulose when subjected to drying, i.e. hornification (Idström et al. 2013; Laivins and Scallan 1993; Newman 1998). Hornification of regenerated cellulose when subjected to drying/wetting cycles has also been confirmed in a recent study (Široká et al. 2012).

By using the method described in "Solid-state NMR spectroscopy", the crystallinity index was calculated on the samples coagulated in water and exposed to the different drying conditions. An indication of increased CI could be seen in the solid-state NMR spectra in Fig. 3, as an increase of crystalline signal intensity and a decrease of non-crystalline signal intensity, with increased drying conditions. However, the CI-values obtained did not give an unambiguous trend, as can be seen in Table 2. The major increase was seen between never-dried films and films treated by any type of drying, whereas by comparing the various drying procedures only minor changes were found. For films coagulated in EtOH and PrOH, only a small fraction of crystalline cellulose was found, giving a very low CI.

A similar trend as for samples coagulated in water was also seen for the samples coagulated in EtOH and PrOH after being subjected to the same drying procedures. The solid-state NMR spectra of the films coagulated in PrOH and exposed to the drying conditions can be seen in Fig. 4. An increase of crystalline signal intensity (a and b) at 89.3 and 88.1 ppm and an apparent decrease of non-crystalline signal intensity (c and d) at 86.6 and 85.1 ppm can be seen, possibly indicating the occurrence of a hornification-like process also in these samples. However, due to the low crystalline amount in this sample it was not possible to distinguish the surface signals from the broad non-crystalline signal and hornification could therefore not be proved. A similar trend was seen also for samples coagulated in EtOH when treated to the same drying procedures (see Appendix Fig. 7).

Table 2 Crystallinity index (CI) for the H_2O-coagulated films

Sample	CI
H_2O ND	0.69
H_2O 75 % RH	0.75
H_2O 11 % RH	0.76
H_2O OD	0.78
H_2O 5 × OD	0.78

NMR cryoporometry

While a true pattern of pore size distribution as a function of pore radius is directly given by the melting (or freezing) curve from cryoporometry, the absolute pore radii can only be calculated for known pore geometry. The pore geometry is normally determined experimentally by combining the recorded freezing and melting curves and choosing the pore geometry model that give the best fit to the data (Petrov and Furó 2009). For gel-like cellulose-based structures such as the water-swollen cell wall of pulp and pharmaceutical coatings of substituted cellulose, we have previously found that cavities of spherical shape (i.e. higher curvature) is the most suitable pore geometry for the pores in the nanometer to micrometer range of hydrogels (Boissier et al. 2012; Östlund et al. 2010). In this study we therefore, and for all samples, assume spherical pore geometry for the calculation of the pore size distribution (PSD) Moreover, only small pores with radii between 2 and 60 nm were quantified, where most pores showed a significant distribution below pore radius of 15 nm as illustrated in Fig. 5 for films coagulated in H_2O. Above $r = 60$ nm the measurements are not as accurate for all samples due to unexpectedly long melting periods, which generates non-total melting of water in the corresponding pore regimes.

Several informative features were observed from the plot of the PSD (Fig. 5). First, the majority of the detected pores were smaller than 15 nm, other significant porous structures were concluded to be above 60 nm in size though they were not studied in this work. Second, a bimodal distribution pattern, as visible in Fig. 5, was shown by the films dried according to ND, 75 % RH, 11 % RH, and OD respectively. The two distinct maxima of this distribution were located at approximately 3 nm and 5 nm. For the film denoted 5 × OD, the PSD showed only one maximum at around 3 nm. Third, the total amount of small pores increased as a function of drying procedure as ND < 75 % RH < 11 % RH < OD. This trend was noticeable for both maxima in the PSD. The 5 × OD film had a decreased total amount of small pores compared to the OD film.

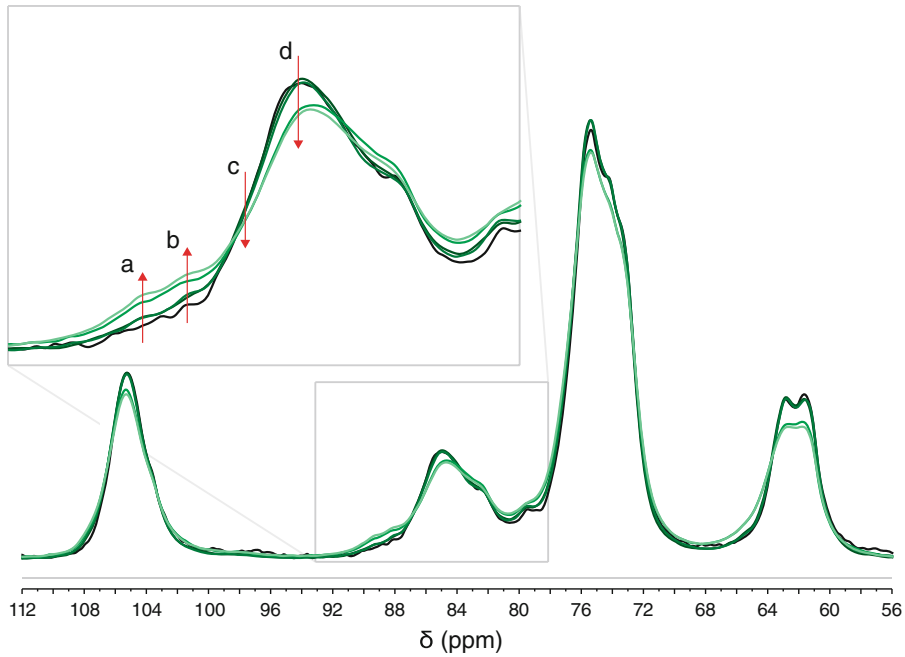

Fig. 4 Solid-state CP/MAS ^{13}C NMR spectra of the films coagulated in PrOH. ND (*black*), 75 % RH (*very dark green*), 11 % RH (*dark green*), OD (*green*), and 5 × OD (*light green*). The C-4 region is enlarged and the *arrows* are highlighting the turnover of the spectra. (Color figure online)

Figure 6 shows the PSD of the films coagulated in PrOH and it is also representative for the PSD of the films coagulated in EtOH (see Fig. 8 in "Appendix"). The bimodal PSD is apparent also for cellulose coagulated in EtOH and PrOH. Notably, the distribution is stretched towards larger pore sizes compared to that of films coagulated in H_2O. The bimodal PSD was observed regardless of coagulation medium, in agreement with the work of Isobe et al. (2011). In their study, cellulose was dissolved in LiOH/urea and coagulated in five different coagulation media with different polarities. In our study, similar to the films with H_2O as coagulation medium, the films coagulated in PrOH showed a collapse of pores larger than 5 nm,

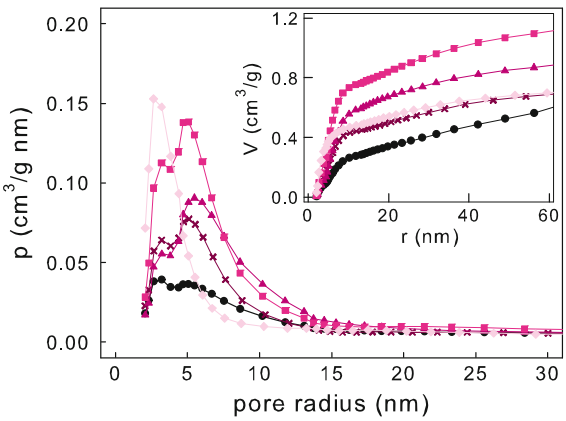

Fig. 5 The nanometer pore size distribution of films coagulated in H_2O: ND (*black circles*), 75 % RH (*violet crosses*), 11 % RH (*dark pink triangles*), OD (*pink squares*), and 5 × OD (*light pink diamonds*). The accumulated pore volume is shown as an *inset*. (Color figure online)

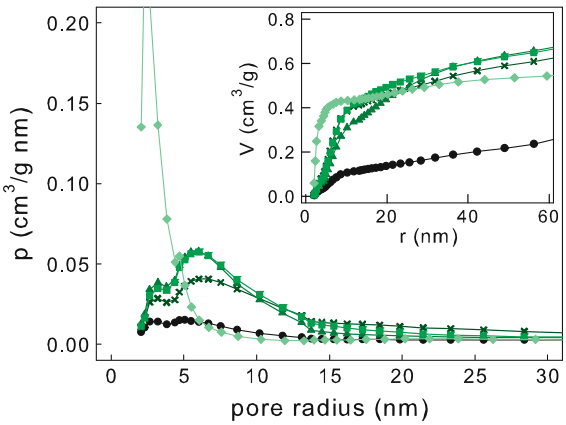

Fig. 6 The nanometer pore size distribution of the PrOH-coagulated films: ND (*black circles*), 75 % RH (*very dark green crosses*), 11 % RH (*dark green triangles*), OD (*green squares*), and 5 × OD (*light green diamonds*). The accumulated pore volume is shown as an *inset*. (Color figure online)

though remarkably the bimodal PSD was shown to change into a mainly monomodal PSD after 5 times repeated wetting and oven-drying (Fig. 6).

Concluding, the results from Figs. 5 and 6, an increase of small pores can be seen when treating the films according to the drying processes in Table 1. A bimodal pattern with pores at 3 and 5 nm can be seen for all films except after the hardest drying treatment only the smallest pores remain. This behavior in PSD pattern with respect to drying method was found for the PSD of the all three coagulants, H_2O, EtOH, and PrOH. If we regard the possibility that different coagulation and drying methods may result in different pore geometries, one should note that the size distribution pattern would still remain the same and only the radii value on the x-axis would be altered.

Pore collapse and crystallization

From the results of PSD (in Figs. 5 and 6) one can follow a trend to larger amount of small pores by drying the samples. This could imply that a restructuring of the cellulosic structure occurs as larger pores ($r > 60$ nm) in the hydrogel films collapses are responsible for the generation of an increased amount of smaller pores ($r < 15$ nm). This behavior is connected to the drying conditions where less humidity and more heat enhances the restructuring. During cyclic oven-drying and rewetting, small pores ($5 < r < 15$ nm) collapse even further, resulting in a monomodal PSD centered around 3 nm. This trend was observed for all films investigated in this study independent of CI. In parallel to our results, Liu et al. have shown that cellulose films (from 10 % cellulose in EMIMAc) coagulated in H_2O show significantly lower water-permeability compared to films prepared in EtOH as a coagulant, which also indicates a more dense microstructure in the total pore regime for H_2O coagulated cellulose films (Liu and Budtova 2012).

Combining the results from cryoporometry with those from solid-state NMR for films coagulated in H_2O, we can conclude that during pore collapse the cellulose simultaneously undergoes an apparent increased crystallization. A probable co-crystallization between cellulosic fibrils is one possible explanation for this, as referred to in "Impact of drying". Hence, both porosity and crystallinity have the potential to be tuned during the regeneration process by choosing an appropriate coagulation medium and subsequent drying. The coagulation of the cellulose from the EMIMAc solution is governed by the miscibility of the ionic liquid in the coagulation medium and the polarity of the coagulation medium. Higher polarity ($H_2O > EtOH > PrOH$) favors the aggregation of cellulose. It is here suggested to occur as a result of better miscibility between EMIMAc and coagulant with higher polarity in combination with the effect of hydrophobic interactions of glucose ring.

Conclusions

From the studies it was concluded that both the coagulation medium and the post-treatment influence the regenerated cellulose films. A complete conversion from cellulose I can be seen for all coagulation media (H_2O, EtOH, and PrOH) ranging from mainly crystalline cellulose II after coagulation in water, to a mainly non-crystalline structure after coagulation in an alcohol.

After drying of the regenerated cellulose films coagulated in water, hornification was seen in the form of an increase of NMR signals originating from crystalline interiors and a corresponding decrease of signals from cellulose crystal surfaces. An apparent increased crystallinity was seen for all samples in the study. A bimodal pore size distribution with pore size maxima of 3 and 5 nm was seen for samples exposed to all but the harshest drying treatment, which showed a monomodal pore size distribution, centered around 3 nm pores.

It was concluded that porosity and crystallinity is more tunable for a cellulose hydrogel coagulated in water than for corresponding gels coagulated in alcohols. However, further research has to be performed in order to get a more thorough picture on how cellulosic materials can be produced to reach controlled porosity at various pore size distributions.

Acknowledgments This work has been carried out within the framework of Avancell—Centre for Fibre Engineering. Financial support from the Swedish Foundation, Södra Skogsägarnas stiftelse för forskning, utveckling och utbildning, and Chalmers Area of Advance Material Science are all gratefully acknowledged. The NMR measurements were carried out at the Swedish NMR Centre, Göteborg, Sweden. Dr. Derek Weightman at Sappi Saiccor in South Africa is kindly acknowledged for supplying samples of the eucalyptus dissolving pulp.

Appendix

See Figs. 7 and 8.

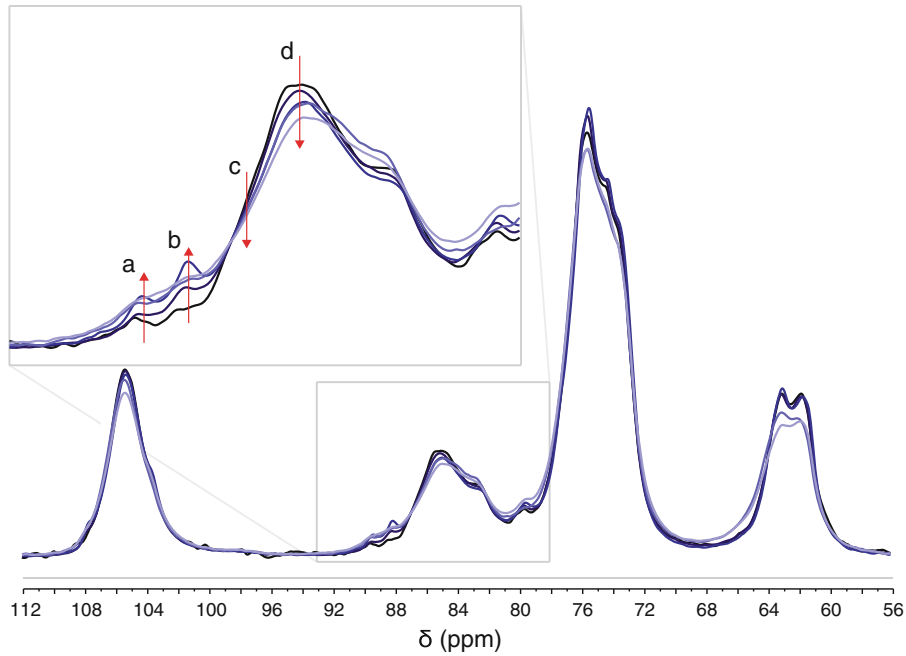

Fig. 7 Solid-state CP/MAS ^{13}C NMR spectra of the films coagulated in EtOH. ND (*black*), 75 % RH (*very dark blue*), 11 % RH (*dark blue*), OD (*blue*), and 5xOD (*light blue*). The C-4 region is enlarged and the *arrows* are highlighting the turnover of the spectra. (Color figure online)

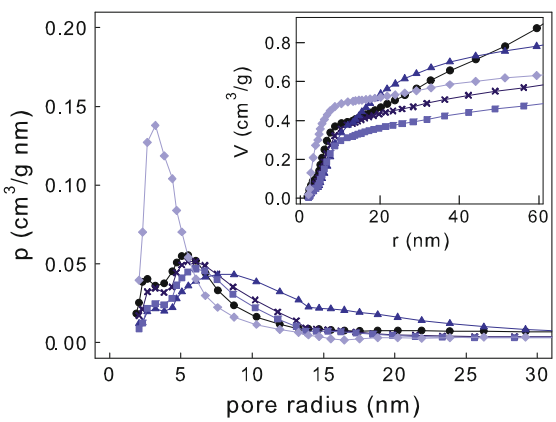

Fig. 8 The nanometer pore size distribution of the EtOH-coagulated films: ND (*black circles*), 75 % RH (*very dark blue crosses*), 11 % RH (*dark blue triangles*), OD (*blue squares*), and 5 × OD (*light blue diamonds*). The accumulated pore volume is shown as an *inset*. (Color figure online)

References

Biganska O, Navard P (2005) Kinetics of precipitation of cellulose from cellulose−NMMO−water solutions. Biomacromolecules 6:1948–1953

Biganska O, Navard P (2009) Morphology of cellulose objects regenerated from cellulose–N-methylmorpholine N-oxide–water solutions. Cellulose 16:179–188

Boerstoel H, Maatman H, Westerink JB, Koenders BM (2001) Liquid crystalline solutions of cellulose in phosphoric acid. Polymer 42:7371–7379

Boissier C, Feidt F, Nordstierna L (2012) Study of pharmaceutical coatings by means of NMR cryoporometry and sem image analysis. J Pharm Sci 101:2512–2522

Cousins SK, Brown RM Jr (1995) Cellulose I microfibril assembly: computational molecular mechanics energy analysis favours bonding by van der Waals forces as the initial step in crystallization. Polymer 36:3885–3888

French AD, Miller DP, Aabloo A (1993) Miniature crystal models of cellulose polymorphs and other carbohydrates. Int J Biol Macromol 15:30–36

Ibbett RN, Domvoglou D, Fasching M (2007) Characterisation of the supramolecular structure of chemically and physically modified regenerated cellulosic fibres by means of high-resolution carbon-13 solid-state NMR. Polymer 48:1287–1296

Idström A, Brelid H, Nydén M, Nordstierna L (2013) CP/MAS 13C NMR study of pulp hornification using nanocrystalline cellulose as a model system. Carbohydr Polym 92:881–884

Isobe N, Kim U-J, Kimura S, Wada M, Kuga S (2011) Internal surface polarity of regenerated cellulose gel depends on the species used as coagulant. J Colloid Interface Sci 359:194–201

Isobe N, Kimura S, Wada M, Kuga S (2012) Mechanism of cellulose gelation from aqueous alkali-urea solution. Carbohydr Polym 89:1298–1300

Kotek R (2006) Regenerated cellulose fibers. In: Lewin M (ed) Handbook of fiber chemistry, 3rd edn. Taylor & Francis, CRC Press, New York, USA, pp 668–764

Laity PR, Glover PM, Hay JN (2002) Composition and phase changes observed by magnetic resonance imaging during non-solvent induced coagulation of cellulose. Polymer 43:5827–5837

Laivins GV, Scallan AM (1993) The mechanism of hornification of wood pulps. In: Baker CF (ed) Products of papermaking, Trans 10th Fund Res Symp, Oxford, pp 1235–1260

Larsson PT, Wickholm K, Iversen T (1997) A CP/MAS13C NMR investigation of molecular ordering in celluloses. Carbohydr Res 302:19–25

Lindman B, Karlström G, Stigsson L (2010) On the mechanism of dissolution of cellulose. J Mol Liq 156:76–81

Liu W, Budtova T (2012) Ionic liquid: a powerful solvent for homogeneous starch–cellulose mixing and making films with tuned morphology. Polymer 53:5779–5787

Liu H, Cheng G, Kent M, Stavila V, Simmons BA, Sale KL, Singh S (2012) Simulations reveal conformational changes of methylhydroxyl groups during dissolution of cellulose Iβ in ionic liquid 1-ethyl-3-methylimidazolium acetate. J Phys Chem B 116:8131–8138

Mori T, Chikayama E, Tsuboi Y et al (2012) Exploring the conformational space of amorphous cellulose using NMR chemical shifts. Carbohydr Polym 90:1197–1203

Newman RH (1998) Evidence for assignment of 13C NMR signals to cellulose crystallite surfaces in wood, pulp and isolated celluloses. Holzforsch 52:157–159

Newman RH (2004) Carbon-13 NMR evidence for co crystallization of cellulose as a mechanism for hornification of bleached kraft pulp. Cellulose 11:45–52

Newman RH, Davidson TC (2004) Molecular conformations at the cellulose–water interface. Cellulose 11(1):23–32

Nocanda X, Larsson PT, Spark A, Bush T, Olsson A, Madikane M, Bissessur A, Iversen T (2007) Cross polarisation/magic angle spinning 13C-NMR spectroscopic studies of cellulose structural changes in hardwood dissolving pulp process. Holzforsch 61:675–679

Östlund Å, Köhnke T, Nordstierna L, Nydén M (2010) NMR cryoporometry to study the fiber wall structure and the effect of drying. Cellulose 17:321–328

O'Sullivan AC (1997) Cellulose: the structure slowly unravels. Cellulose 4:173–207

Park S, Johnson D, Ishizawa C, Parilla P, Davis M (2009) Measuring the crystallinity index of cellulose by solid state 13C nuclear magnetic resonance. Cellulose 16:641–647

Park S, Baker J, Himmel M, Parilla P, Johnson D (2010) Cellulose crystallinity index: measurement techniques and their impact on interpreting cellulase performance. Biotechnol Biofuels 3:10

Petrov OV, Furó I (2009) NMR cryoporometry: principles, applications and potential. Prog Nucl Magn Reson Spectrosc 54:97–122

Sescousse R, Gavillon R, Budtova T (2011) Aerocellulose from cellulose–ionic liquid solutions: preparation, properties and comparison with cellulose–NaOH and cellulose–NMMO routes. Carbohydr Polym 83:1766–1774

Široká B, Manian AP, Noisternig MF et al (2012) Wash–dry cycle induced changes in low-ordered parts of regenerated cellulosic fibers. J Appl Polym Sci 126:E397–E408

Yang Q, Fujisawa S, Saito T, Isogai A (2012) Improvement of mechanical and oxygen barrier properties of cellulose films by controlling drying conditions of regenerated cellulose hydrogels. Cellulose 19:695–703

Zhang S, Li FX, Yu JY (2010) Structure and properties of novel cellulose fibres produced from NaOH/PEG-treated cotton linters. Iran Polym J 19:949–957

Ziabicki A (1976) Fundamentals of fibre formation: the science of fibre spinning and drawing. Wiley, Minnesota, USA

Zuckerstätter G, Schild G, Wollboldt P, Roeder T, Weber HK, Sixta H (2009) The elucidation of cellulose supramolecular structure by 13C CP-MAS NMR. Lenzing Ber 87:38–46

Zuckerstätter G, Terinte N, Sixta H, Schuster KC (2013) Novel insight into cellulose supramolecular structure through 13C CP-MAS NMR spectroscopy and paramagnetic relaxation enhancement. Carbohydrat Polym 93:122–128